Fire Detection Using GOES Rapid Scan Imagery

JOHN F. WEAVER, DAN LINDSEY, AND DAN BIKOS

NOAA/NESDIS/RAMM Team, Cooperative Institute for Research in the Atmosphere, Colorado State University, Fort Collins, Colorado

CHRIS C. SCHMIDT

Cooperative Institute for Meteorological Satellite Studies, Madison, Wisconsin

ELAINE PRINS

NOAA/NESDIS/ORA/ARAD Advanced Satellite Products Team, Madison, Wisconsin

(Manuscript received 28 July 2003, in final form 3 November 2003)

ABSTRACT

This paper demonstrates the proper use of geostationary satellite imagery in wildland fire detection. The roles of both the visible and the 3.9-μm channels are emphasized. Case studies from June 2002 are presented to illustrate techniques that can be utilized in both the detection and short-range forecasting processes. The examples demonstrate that, when utilized correctly, the sensitivity of the shortwave infrared channel to subpixel heat sources can often result in detections that match the timelines of human observations. Finally, a derived satellite product that increases the detection rate of wildland fires from space is described.

1. Introduction

For most of the United States, timely detection of wildland fires relies almost entirely on human spotter reports. However, when utilized correctly, satellite imagery provides supplementary detection information that can be particularly valuable at night, or where human presence is sparse. Though polar-orbiting satellites [e.g., *National Oceanic and Atmospheric Administration-17* (*NOAA-17*), Defense Meteorological Satellite Program (DMSP), Moderate Resolution Infrared Spectroradiometer (MODIS)] have instrumentation that can detect fires with flame fronts as small as 0.0015 km^2, these instruments are limited by the fact that polar-orbiting satellites make infrequent passes over the same spot on Earth each day. Routine, 15-min-interval scans are available from geostationary satellites, but until recently the spatial resolution of these data has been considered too coarse to be useful. Using several examples from the summer of 2002, we will show that this is not entirely true.

The year 2002 was marked by severe drought across most of the Rocky Mountain west (Fig. 1). Fuel moisture contents were at record low levels in many areas. In Colorado, there had been 10 wildland fires by 7 June, each of which had burned areas on the order of 10^2–10^3 acres (1 acre $\simeq$ 0.4 ha). The National Weather Service (NWS) Denver/Boulder Forecast Office had issued 11 ''red flag'' warnings (extreme fire danger) by early June, which is four times the normal for that early in the year. NWS fire weather meteorologists, U.S. Forest Service personnel, and state and county agencies were all warning that the fire situation would worsen as the drought wore on. In fact, the year 2002 turned out to be the worst wildland fire season in Colorado recorded history.

As the fire threat was becoming progressively worse, a meteorological research field program, the International H_2O Project (IHOP), was under way in central Oklahoma. In support of this program, the NOAA/National Environmental Satellite, Data, and Information Service (NESDIS) had agreed to temporarily activate its reserve Geostationary Operational Environmental Satellite, *GOES-11*, which had been stored in orbit awaiting potential failure of either one of the operational GOES instruments (then *GOES-8*[1] and *Goes-10*). The activation period ran from 29 May through 20 June 2002. A special schedule during the 3-week period allowed for data collection at a rate of one imaging scan every 5 min over the entire continental United States. This is three times the normal scan frequency. Thus,

Corresponding author address: John F. Weaver, NOAA/NESDIS/RAMM, CIRA Bldg., Colorado State University, Foothills Campus, Fort Collins, CO 80523.
E-mail: weaver@colostate.edu

[1] The eastern geostationary satellite in place in June 2002, *GOES-8*, has been replaced by *GOES-12*.

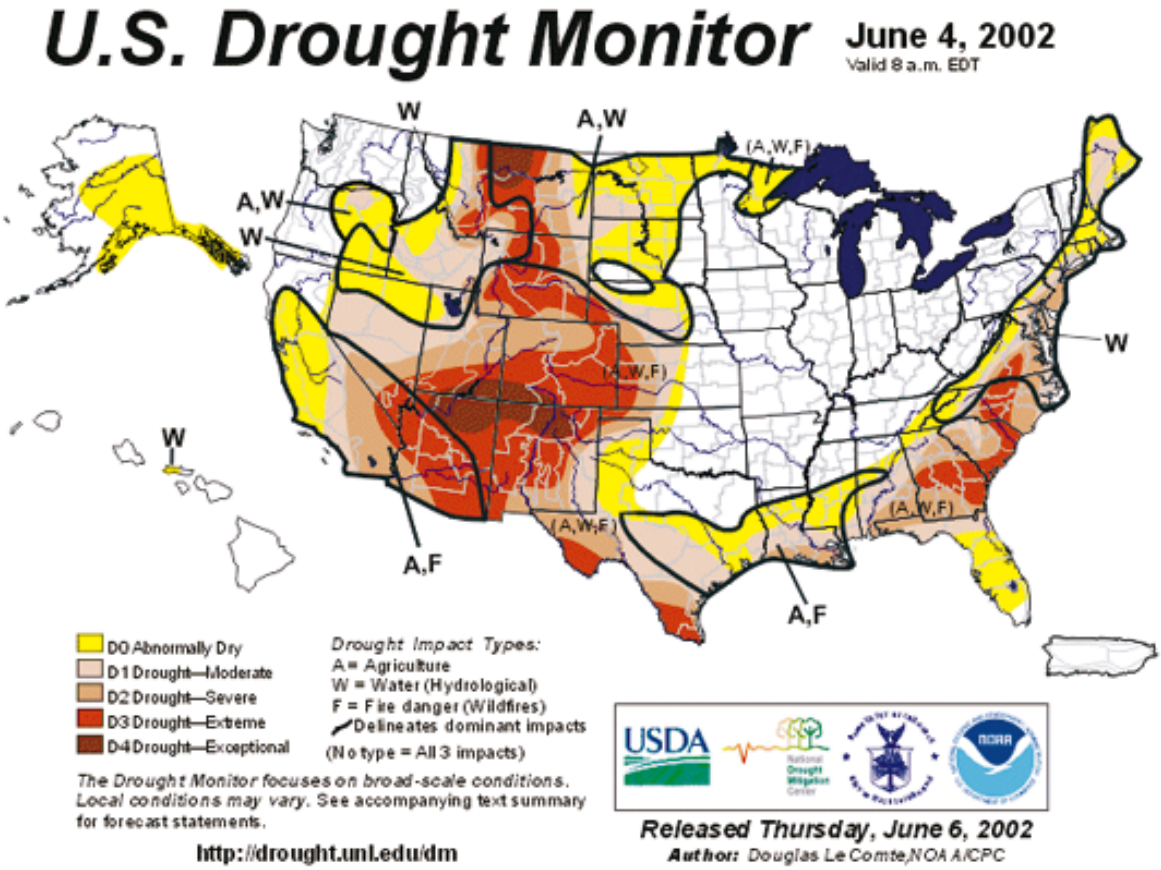

FIG. 1. Map of the United States showing the extent of drought conditions as of 4 Jun 2002. More than half of the western states were experiencing moderate, or greater, drought.

very high time resolution GOES data were being collected on 8–9 June, when five large Colorado forest fires began—two of which turned out to be the two largest in Colorado recorded history. This article describes those 2 days through various datasets, though the discussion is heavily weighted toward 5-min-interval *GOES-11* imagery. It is important to note that current plans are for the next generation of geostationary satellites to carry out routine imaging scans at 5-min intervals.

2. GOES 3.9-μm data

One of the most useful channels for wildland fire detection on all of the GOES imagers is the shortwave infrared channel (sometimes referred to as channel 2), which has a peak response at 3.9 μm (Menzel and Purdom 1994). The 3.9-μm channel is different from the other four imaging channels in that it is characterized by an intense response to subpixel heat (Dozier 1981; Matson and Dozier 1981; Flannigan and Vonder Haar 1986). This strong sensitivity to subpixel heat makes it ideal for use in the early detection of wildland fires (Weaver et al. 1995), especially in forested areas where fires burn hot.

The reason for the more effective subpixel response is evident from Fig. 2a, which portrays Planck radiances for various blackbody temperatures. The shaded bars highlight radiances at shorter, versus longer, infrared wavelengths. The plot illustrates the more rapid change in radiance at shorter versus longer wavelengths as temperature changes occur. Figure 2b compares the *response* of the 3.9-μm channel directly with that of the 10.7-μm channel, a ''window'' channel that senses the actual average near-ground temperature of the pixel being scanned. In this example, the subpixel hot spot is assumed to be 500 K, while the remainder of the area covered by the pixel is at 300 K (i.e., a normal, late spring/early summer day). Note that if only 5% of the pixel is burning at 500 K, the 3.9-μm measured brightness temperature of the pixel is 355 K, while the corresponding 10.7-μm average pixel brightness temperature is about 318 K; that is, the difference between the two responses is substantial. When there is no subpixel heat source in an otherwise clear pixel, or when the entire pixel reaches the 500-K temperature, the two channels are nearly the same, with channel 2 generally running about 2–4 K warmer. The sudden appearance and persistence of a very hot pixel in the 3.9-μm imagery (as compared with nearby pixels) is often an early

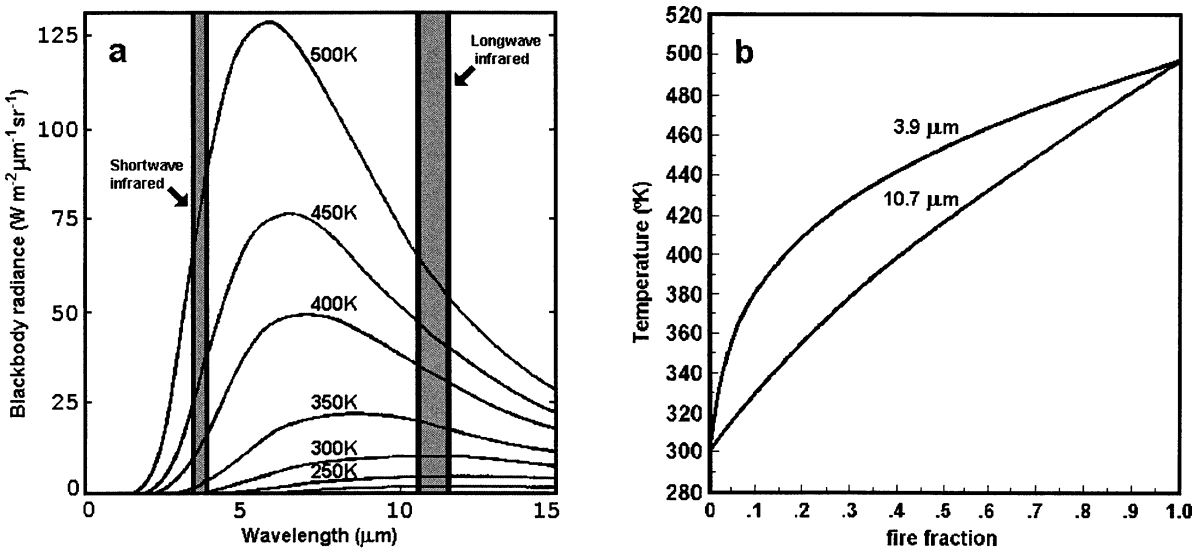

FIG. 2. (a) Comparison of Planck radiances at shorter vs longer infrared wavelengths. The plot illustrates the more rapid response of the shorter wavelengths to increasing heat. (b) Comparison of brightness temperatures in the 3.9- vs 10.7-μm channels for a pixel with a background temperature of 300 K that contains a subpixel heat source of 500 K. Abscissa gives the percentage of the pixel affected by the heat source; ordinate is resulting average pixel brightness temperature (K).

indication of a significant fire. (Note that lack of persistence with time may be a sign of instrument noise, or of a short-lived, prescribed burn.)

It should also be noted that 3.9-μm sensors on the current geostationary satellites ''saturate'' at various temperatures, depending on the satellite. Specifically, these saturation values are as follows: *GOES-10*, 322 K; *GOES-11*, 338 K; and *GOES-12*, 336 K. When utilizing a standard black-to-white enhancement table (wherein warmer brightness temperatures are darker), the saturated pixel will appear black. For *GOES-11*, however, saturated pixels were arbitrarily assigned a value of 163 K. This reassignment was made to allow for experimental calibration testing. Thus, *GOES-11* pixels turn pure white at saturation (e.g., Fig. 3), making fires much easier to spot. When utilizing channel 2 data from the other GOES instruments, the standard linear color table can be adjusted to emulate this feature. However, for the following examples we will be utilizing *GOES-11* data exclusively.

3. The Long Canyon fire—Challenges in scan frequency and data delivery times

The first Colorado wildland fire to appear on 8 June 2002 began about 20 mi northwest of Grand Junction in a wilderness area known as Long Canyon. The cause was determined to be lightning from a weak thunderstorm that had passed over the area on the afternoon of 3 June 2002. Smoldering, partially decomposed organic ground cover (known as duff) flared into an active wildland fire when strong, midlevel winds mixed down to the surface and began gusting from the southwest—directly into the canyon. The first report of a fire was phoned in to the Grand Junction Bureau of Land Management Fire Protection District dispatch center, by the public, at 1812 UTC. Of interest to this discussion is the fact that the fire could actually be seen as a hot spot on the *GOES-11* 3.9-μm image beginning at 1803 UTC (Fig. 3b), though it may have easily gone unnoticed at the time since the single darkened pixel was located in a region where neighboring pixels were only 6°–11°C cooler. A small sampling among a number of Cooperative Institute for Research in the Atmosphere (CIRA) researchers suggests that a darkened pixel becomes ''visually evident'' when the temperature difference between a 3.9-μm counterpart is in the range of 10°–15°C. Thus, the fire-involved pixel in this image was very close to the limit of perception. Apart from the fire meteorologist's perceptive ability, however, there are other factors that work against the utility of this potentially powerful tool. The two most important of these are scan frequency and delays in data delivery.

The first factor that can adversely affect efficient use of the data is scan frequency. Under the current routine-operations scanning schedule, GOES images are collected at an interval of 15 min. In that mode, the first time the hot spot would have become truly obvious would have been at 1815 UTC (Fig. 3c). Going back to 1803 UTC (the closest time to 1800 on the special *GOES-11* schedule), one can identify a darkened pixel in the same location. However, it is prudent to observe a series of two to three images showing a hot pixel in the same location before thinking, ''possible wildland fire.'' In this case—since there is a hot spot in the 1803, 1815, and 1834 UTC images—the fire weather meteorologist can be fairly confident that a wildland fire is in progress shortly after viewing the third image.

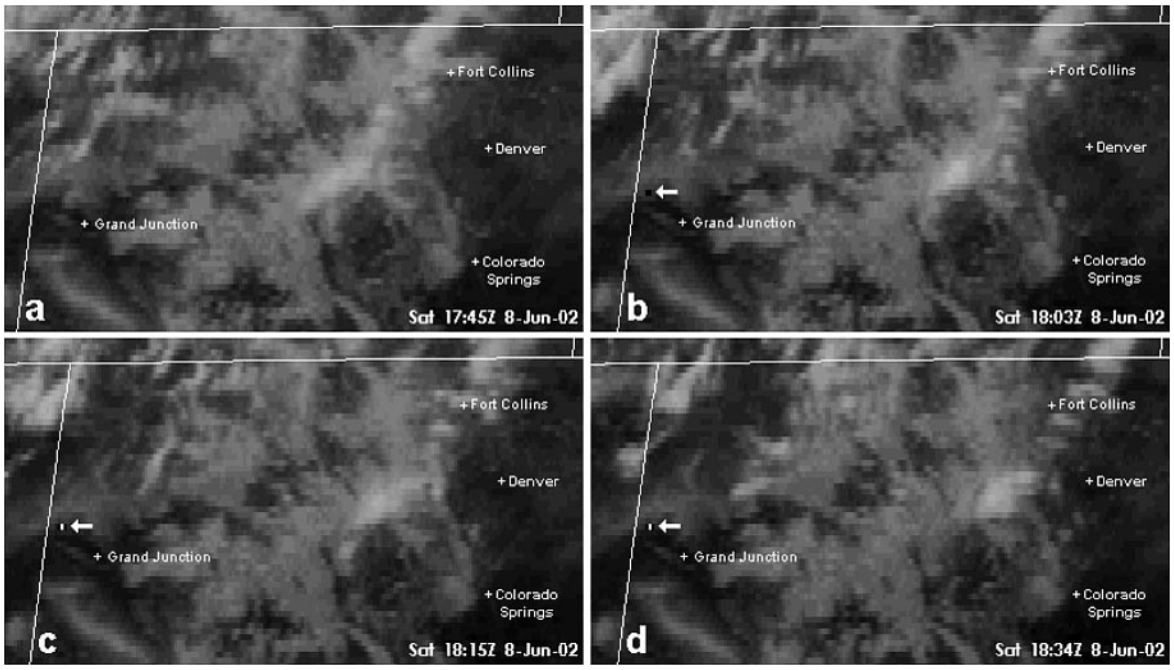

FIG. 3. *GOES-11,* approximate 15-min-interval, channel 2 imagery taken at (a) 1745, (b) 1803, (c) 1815, and (d) 1834 UTC on 8 Jun 2002. Arrow points to bright pixels associated with the Long Canyon, CO, wildland fire. Images would be available on AWIPS at approximately 1802, 1825, 1837, and 1856 UTC, respectively. The cities of Grand Junction, Fort Collins, Denver, and Colorado Springs are shown for reference points.

This brings us to the second issue; that of delayed data delivery. Under the present routine operational schedule, satellite images are not loaded onto the NWS forecaster's data display system (Advanced Weather Interactive Processing System; AWIPS) until about 20–25 min after initial scan time (AWIPS design requirements specify a maximum delay time of 25 min). Thus, the fire weather meteorologist would not generally be able to obtain the requisite series of three images until about 1854–1859 UTC, or 42–47 min after the fire was first reported by the public.

Data delivery occurs more rapidly when rapid scan operations (RSO) are taking place. RSO is a special imaging schedule that can be activated by any National Weather Service office for any situation it deems necessary. The RSO schedule doubles the number of images received each hour, and transfers the imagery onto AWIPS nearly three times more quickly. Design specifications call for RSO imagery to be delivered to the AWIPS within 8 min of initial scan time.

Now consider the *GOES-11,* 5-min-interval imagery (Fig. 4), which was operated during IHOP under RSO scheduling guidance. Even if one did not notice the warm pixel(s) at 1803 and 1807 UTC, the saturated pixel at 1815 UTC is quite evident. After noticing the fire at 1815, one could revisit the 1803 and 1807 images, and find the overheated spot. This series of three images provides some confidence that one is looking at an actual wildland fire—the decision to report the fire could be made as soon as the 1815 image is delivered to AWIPS. In this case, since the *GOES-11,* 5-min data were collected within RSO guidelines, information that a wildland fire was in progress was available within 12 min of the first public report of the fire. In less populated regions, or at night, GOES-RSO imagery can often be the first indication of a fire.

Future GOES systems are planned that allow for routine rapid-interval scanning schedules (5-min scanning is planned for GOES-R) at twice the spatial resolution of today's satellites. Furthermore, future display systems include plans for more rapid delivery of imagery, so lead times will be cut even further. However, current RSO scheduling represents a partial solution that is available now. Though today's rapid-scan schedule operates at an uneven imaging interval mode due to conflicting scheduling obligations (see Table 1), the delivery time to the AWIPS is still around 8 min. During fire season, it is strongly recommended that fire weather meteorologists call for RSO on days when red flag warnings are in effect.

4. A late detection and a prescribed burn

According to a Garfield County, Colorado, press release, a fire that came to be known as the Coal Seam fire was first reported at about 1900 UTC on 8 June 2002. It eventually burned more than 12 000 acres, and destroyed 43 structures (29 homes and 14 outbuildings) in and around the town of Glenwood Springs, Colorado. The fire was started by an underground coal seam that

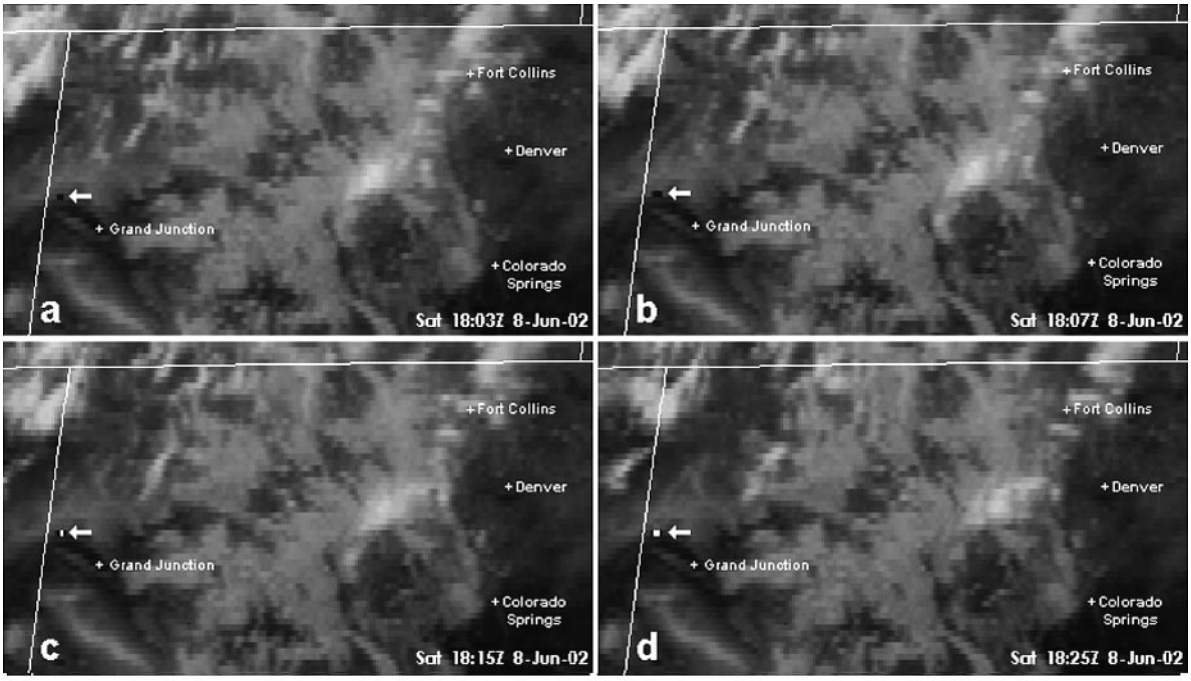

FIG. 4. *GOES-11*, 5-min-interval, channel 2 imagery taken at (a) 1803, (b) 1807, (c) 1815, and (d) 1825 UTC on 8 Jun 2002. Arrow points to bright pixels associated with the Long Canyon wildland fire. Images would be available on AWIPS at approximately 1811, 1815, 1823, and 1833 UTC, respectively. The cities of Grand Junction, Fort Collins, Denver, and Colorado Springs are shown for reference points.

had been burning for more than 25 yr. Over the first 45 min of its life the fire grew appreciably in size and at 1945 UTC Glenwood Springs firefighters requested helicopter support. By that time, the fire had burned a narrow swath nearly a mile long. However, the fuel type involved during these early stages was primarily dry grass with scattered brush. Grasslands tend to burn at roughly half the temperature of densely shrubbed or forested areas (Bailey and Anderson 1980), and grass fires often advance with very thin, narrow fire fronts. Thus, the subpixel heat was insufficient to show up on the *GOES-11* channel 2 imagery (Fig. 5). Though darkened pixels could be seen off and on during the first couple of hours, it was not until later in the afternoon that pixels became saturated in the imagery. It is clear that detection of the Coal Seam fire by satellite would have lagged the public report by at least an hour. This is to be expected for wildland fires involving short grass. Remember that before a darkened pixel becomes visually evident, the temperature difference between the 3.9- and 10.7-μm pixels must be roughly 10°–15°C. This difference represents an involvement of about 2% of the pixel area for $\Delta T = 200$ K (Figs. 2 and 6), which is the temperature *difference* used for the example illustrated in Fig. 2. For a 2.4 km $\times$ 5.9 km pixel (which is the pixel size for ~3500 acres during this period)—the pixel size for *GOES-11* 3.9-μm imagery at the latitude and longitude of central Colorado during this period—2% would require that around 70 acres be burning vigorously. This 2% threshold also assumes that the fire is not on a steep slope facing away from the satellite, is not burning in underbrush beneath the forest canopy, and that there is not substantial cloud cover. The better resolution planned for future GOES instruments will allow detection of much smaller fires. With the resolution planned for these instruments, the infrared pixel size will be roughly 875 acres and the active burn area would only have to be about 15 acres in the present example.

TABLE 1. Example of hourly data collection schedule used for GOES rapid-scan operations.

Start time (UTC)	Region scanned	Scan duration (min:s)
1902:11	Continental United States	4:43
1910:00	Continental United States	4:43
1915:00	Northern Hemisphere	9:44
1925:00	Continental United States	4:43
1930:00	Southern Hemisphere (small winds)	1:45
1932:11	Continental United States	4:43
1940:00	Continental United States	4:43
1945:00	Northern Hemisphere	9:44
1955:00	Continental United States	4:43

Another factor that could have represented a distraction from the Coal Seam fire was a prescribed burn taking place in Eagle County (Fig. 5). That fire was hot enough to darken a pixel or two for several scans. The signal might easily have diverted the fire weather meteorologist's attention from less obvious signals, or per-

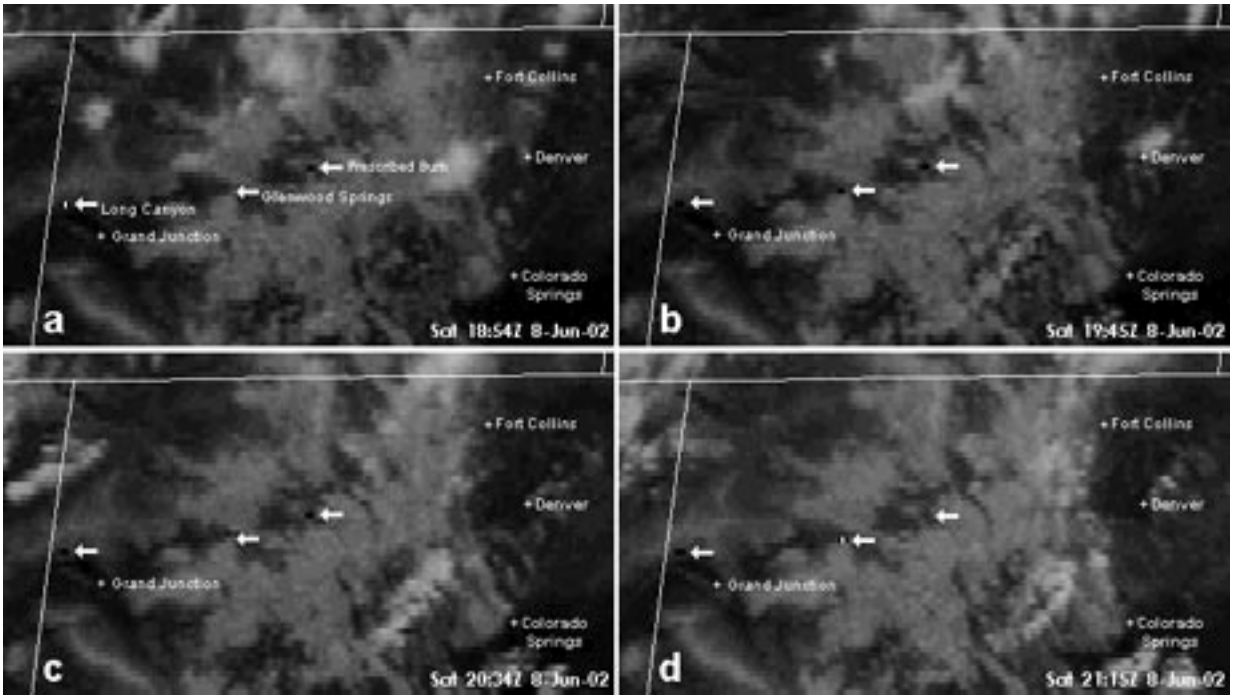

FIG. 5. *GOES-11* channel 2 imagery taken at (a) 1854, (b) 1945, (c) 2034, and (d) 2115 UTC on 8 Jun 2002. Arrows point to the Long Canyon fire, Glenwood Springs (the Coal Seam fire originates just west of there), and the prescribed burn in Eagle County (left to right, respectively). The cities of Grand Junction, Fort Collins, Denver, and Colorado Springs are shown for reference points.

haps even led to a false alarm, had there been no prior notification of the prescribed burn. However, most fire weather meteorologists are aware of prescribed burns in their warning areas. Furthermore, even if a false alarm had occurred, it most likely would not have been considered a serious problem. It is becoming increasingly clear that emergency managers and responders would prefer receiving a number of false alarms, rather than risk missing the early stages of even one significant fire.

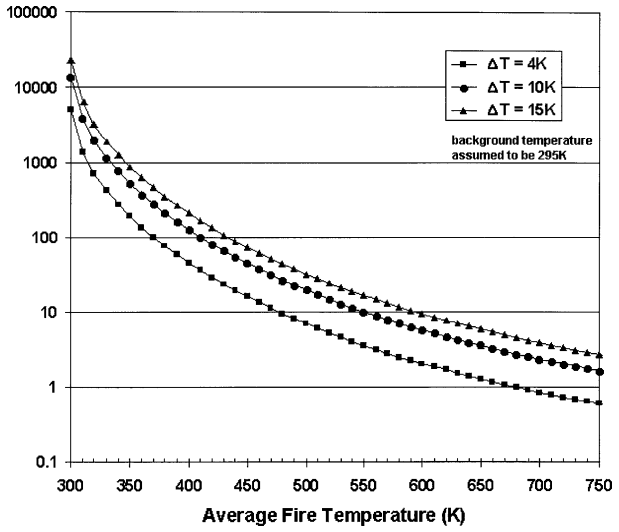

FIG. 6. Graph showing minimum detectable fire size (in acres) vs fire temperature (K) for a *GOES-11*, channel 2 pixel at 40°N. The curves plotted show the relationships for pixels with subpixel fires burning at various temperatures. The curves represent brightness temperatures that are 4, 10, and 15 K hotter than surrounding nonfire pixels at an assumed brightness temperature of 295 K (22°C).

5. The Hayman fire

A fire that was to burn 137 760 acres of Colorado forest, and would eventually destroy 133 private homes, one business, and 466 outbuildings, began late on the afternoon of 8 June 2002. The first spotter report was received at 2255 UTC. It was called in by the person who started it, while it was still just an acre or two in size. On satellite imagery, the effects did not become obvious until around 2345 UTC (Fig. 7). The visible imagery shows that a field of altocumulus clouds had developed over the area (Fig. 8) making the small smoke plume difficult to identify. The 3.9-μm signal was fairly weak during the first hour of the fire for this reason, but interestingly, this signal is continuous. Significant cloud cover is not very common on days when red flag warnings are in effect, especially on very dry days when plume-driven fires are likely. However, when cloudiness does occur, detection of wildland fires by geostationary satellite can be delayed. Another instance when cloudiness may slow detection are those days on which lightning from a low precipitation thunderstorm starts the fire. In those cases, detection by satellite will be delayed until anvil cirrus clears the area.

FIG. 7. *GOES-11* channel 2 image taken at 2345 UTC on 8 Jun 2002. Arrows point to hotter pixels associated with the Coal Seam and Hayman fires. The cities of Fort Collins, Denver, and Colorado Springs are shown for reference points. Note that the Long Canyon fire (western Colorado) and a large fire in northern New Mexico (known as the Ponil complex) are also visible.

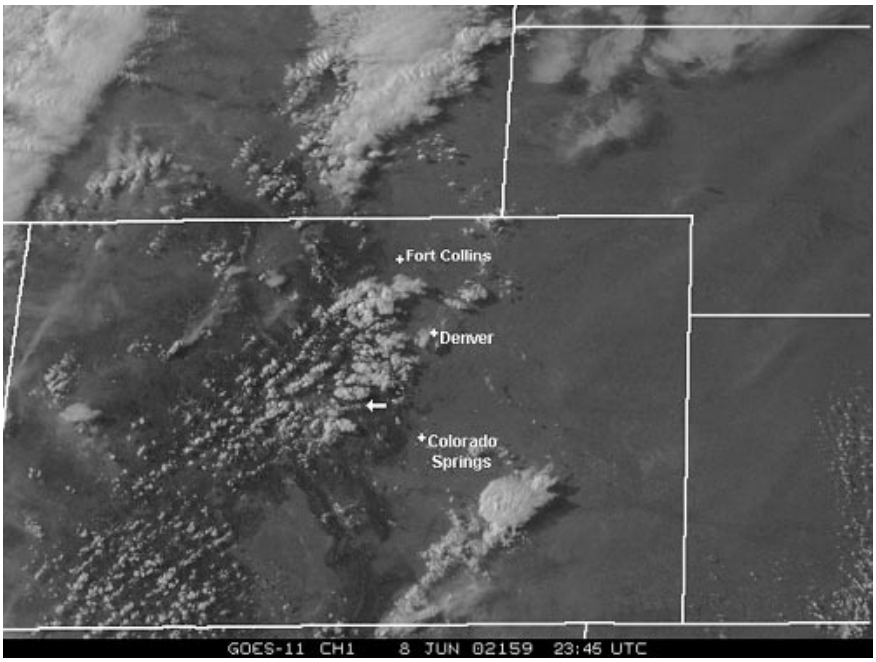

FIG. 8. *GOES-11* visible-wavelength image taken at 2345 UTC on 8 Jun 2002. Arrows point to the partly cloudy Hayman fire area. The cities of Fort Collins, Denver, and Colorado Springs are shown for reference points.

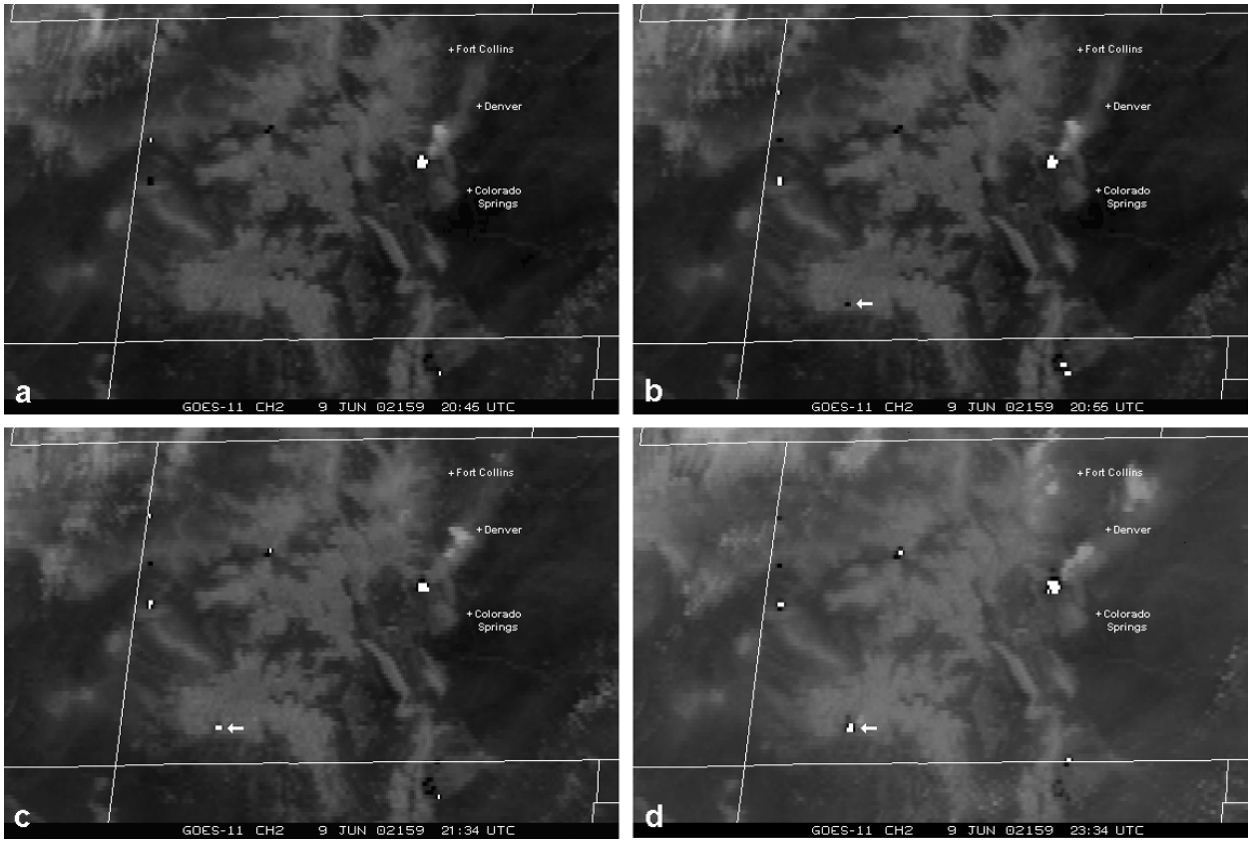

FIG. 9. *GOES-11* channel 2 imagery taken at (a) 2045, (b) 2055, (c) 2134, and (d) 2334 UTC on 9 Jun 2002. Arrow indicates Missionary Ridge fire. The cities of Fort Collins, Denver, and Colorado Springs are shown for reference points.

6. Fires on 9 June 2002—Another large fire and examples of smoke plumes

The last large fire to be discussed in this article will be the Missionary Ridge fire, which started in a ditch beside a roadway, possibly due to a discarded cigarette. It was first reported by the public at 2032 UTC on 9 June 2002. A second fire in western Colorado also began on 9 June, just south of the Long Canyon fire (section 3). This one was named the Dierich fire. Started by an illegal campfire, it burned a total of nearly 3000 acres. It was considered small by 2002 standards. The Missionary Ridge fire, on the other hand, grew very quickly from its inception, destroying 6800 acres of forest land in its first day. By the time the fire was completely contained (on 16 July 2002), it had burned a total of 70 485 acres to become the second largest wildland fire in Colorado recorded history. Detection by satellite in this case was very timely; the first indication of the Missionary Ridge fire on the *GOES-11* imagery came relatively close to the time of the first public report. In fact, the first darkened pixels appeared on the 2050 UTC image (not shown), but were not obvious until 2055 UTC. The fire grew rapidly after that (Fig. 9).

Figure 10 shows a *GOES-11* visible-wavelength view of the four primary Colorado smoke plumes on the late afternoon of 9 June. The Hayman fire plume was extremely large and picturesque on this day. The rising column of hot air was warm enough, and deep enough, to produce large pyrocumulus towers above it (Fig. 11), even though the sounding for that afternoon indicated an extremely dry air mass (Fig. 12). In fact, the convection was sufficiently intense to produce near-precipitation-intensity echoes (Fig. 13). Figure 14 shows the plume in the *GOES-11* visible satellite imagery at the same time. It is easy to distinguish areas of roughly textured cumulus cloudiness from the smoother smoke plumes. Pyrocumulus clouds are indicative of robust, plume-driven fires, which often initiate spot fires off to the side of the primary plume and at a significant angle to the mean mid- and upper-level winds (here, from roughly 230°). In this case, two spot fires formed within 1 h of one another during the afternoon. Note that the visible imagery clearly shows three separate point sources, two of which are spot fires that ignited off to the side of the largest smoke plume.

The extensive, nearly dry adiabatic layer, combined with evidence of the robust fire plume on this day, suggests a deeply mixed smoke layer. Thick, deeply mixed smoke layers can result in a number of problems including air quality issues (Fig. 15) and aviation hazards.

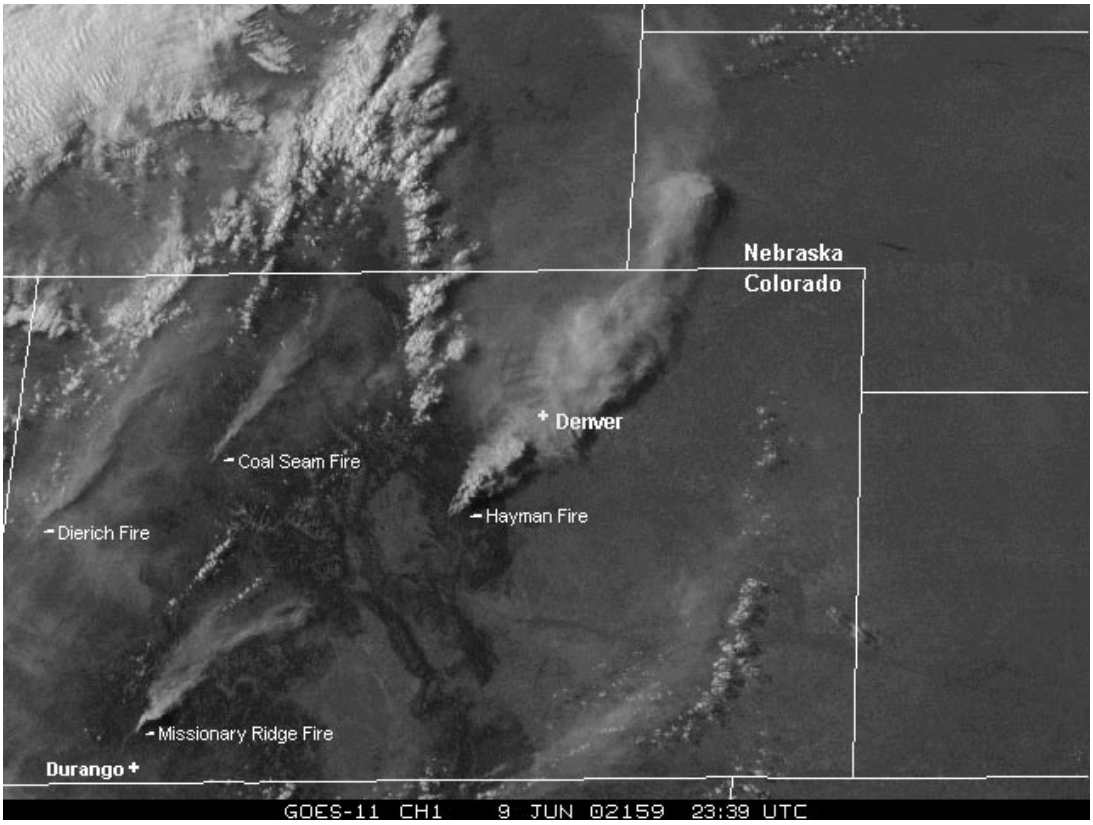

FIG. 10. *GOES-11* visible-wavelength image taken at 2339 UTC on 9 Jun 2002. Arrows point to the four major fires burning at the time. Note the thin smoke plume covering most of the western one-quarter of Colorado. This is smoke from fires burning in Arizona. The Long Canyon fire smoke plume is small and hidden beneath the Arizona smoke.

On this day, Denver International Airport was shut down for nearly 3 h due to limited visibility from the surface to about 34 000 ft MSL.

7. The GOES Wildfire Automated Biomass-Burning Algorithm—WF_ABBA.

The majority of this paper has focused on the use of the standard 3.9-μm imagery in wildland fire detection, simply because of its rapid delivery in AWIPS. There are, however, somewhat more sophisticated methodologies available for fire detection that can be accessed via the Internet. The GOES Wildfire Automated Biomass Burning Algorithm (WF_ABBA) is one such tool. This algorithm was developed to study trends in biomass burning in South America using multispectral GOES sounder data (Prins and Menzel 1992, 1994; Menzel and Prins 1996), and was a derivative of a technique originally developed by Matson and Dozier (1981) for polar-orbiting satellites. The software was recently modified to detect and monitor agricultural and wildfires throughout the Western Hemisphere in near–real time.

The WF_ABBA incorporates statistical techniques to automatically locate and characterize hotter than normal pixels in the GOES imagery using the 3.9-μm, 10.7-μm, and visible imaging bands. Once the algorithm locates a candidate pixel, it utilizes ancillary data to screen for false alarms and correct for water vapor attenuation, surface emissivity, solar reflectivity, and semitransparent cloudiness. Numerical techniques are then applied to determine instantaneous estimates of subpixel fire size and average fire temperature. Results are plotted onto a background map of color-coded land usage. For more information on this algorithm refer to Prins et al. (1998, 2001). ASCII output files that contain information about fire pixels including their location, the observed 3.9- and 10.7-μm brightness temperatures, estimates of instantaneous subpixel fire size and temperature, ecosystem type, and fire classification are also produced by the WF_ABBA. The six fire classification categories are designated as processed pixels (pixels that show indications of subpixel fires), saturated pixels (see section 2), cloudy pixels (a fire pixel with relatively thin cloud cover), high possibility fire pixels, medium possibility fire pixels, and low possibility fire pixels.

The WF_ABBA is currently executed every half hour for both of the operational geostationary satellites. Diurnal animations of large-scale and regional fire composite imagery are posted on the Cooperative Institute for Meteorological Satellite Studies (CIMSS) biomass

FIG. 11. Photograph of the Hayman fire smoke plume on the late afternoon of 9 Jun 2002 taken from a position north of the fire. (Photo courtesy of S. Zufall, U.S. Forest Service.) Note pyrocumulus towers developing above the smoke.

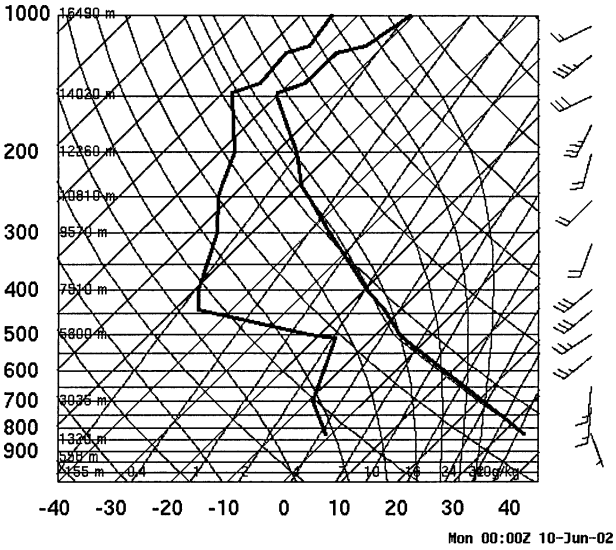

FIG. 12. Radiosonde data from Boulder, CO, valid at 0000 UTC on 10 Jun 2002 plotted on a skew T–log$P$ diagram. Sounding time corresponds to 1800 mountain daylight time (MDT) 9 Jun 2002.

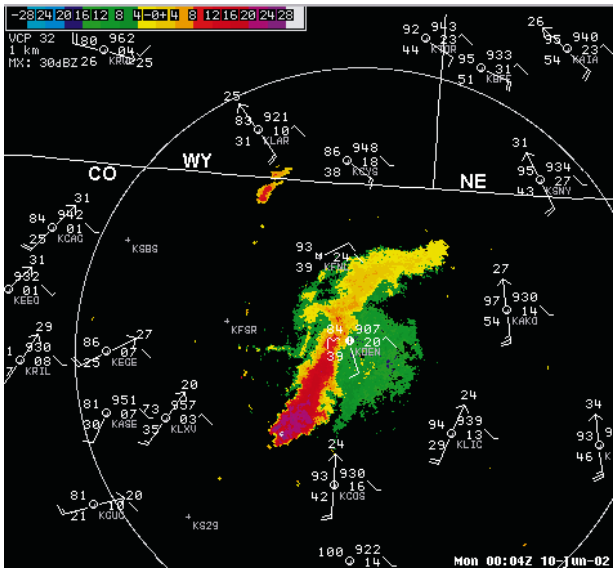

FIG. 13. Radar reflectivity from the Denver, CO, WSR-88D with surface observations superimposed. The large echo to the southwest of Denver (maximum reflectivity 28–30 dBZ) is a result of the Hayman fire plume. Note the observation of smoke over the Denver area. Later that evening, visibility was lowered to 1/4 mi along the entire northern Front Range as the plume expanded.

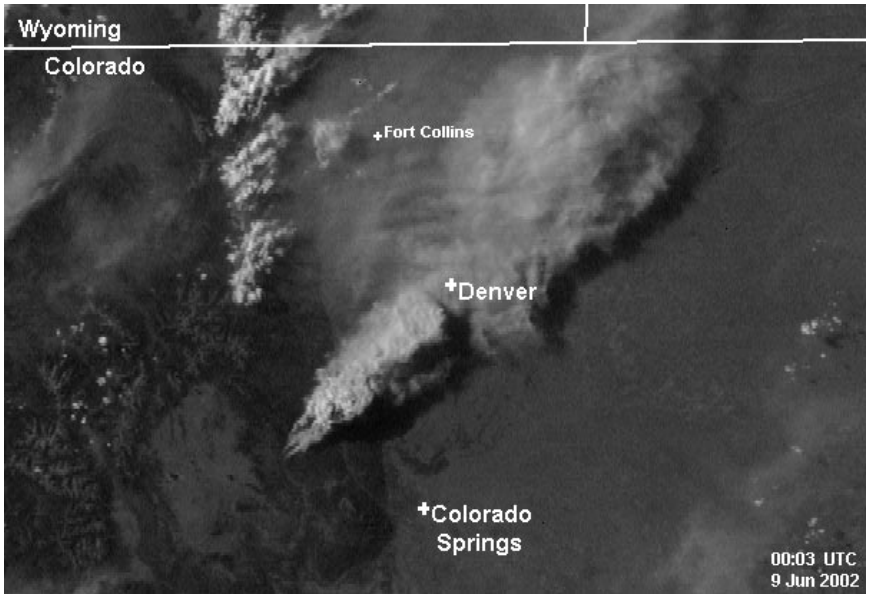

FIG. 14. *GOES-11* visible-wavelength image taken at 0003 UTC on 9 Jun 2002 showing the Hayman fire smoke plume and the associated cumuliform cloudiness ''cap.'' The cities of Fort Collins, Denver, and Colorado Springs are shown for reference points.

burning monitoring Web site (http://cimss.ssec.wisc.edu/goes/burn/wfabba.html), and ASCII files are available via anonymous FTP from the same location. Current delays in real-time posting may be as long as 60 min, though future plans include making WF_ABBA fire products available to the user community within 2–5 min of receiving the GOES imagery. Results from the WF_ABBA can also be found on the NESDIS fire and smoke product Web page (http://www.ssd.noaa.gov/PS/FIRE/hms.html). Here the results are posted about four times more quickly, and are quality controlled by duty meteorologists 7 days a week, 12 h day^{-1}. However, fires are not plotted onto land use maps, nor are ASCII files made available.

Initial evaluation of the WF_ABBA finds that the product has skill in identifying wildfires and distinguishing between fires and highly reflective surfaces (e.g., Prins et al. 2003). The most recent version of the product also has a lower false alarm rate than previous versions. Most mature forest fires burn hotter than the 500-K example presented in section 2. Thus, when we look at hotter fires (e.g., those representing burns within dense shrub or forested areas), the WF_ABBA is able to detect much smaller fires. At the equator, the minimum detectable instantaneous fire size burning at an average temperature of 750 K against a 295-K background under clear-sky conditions is a little more than 0.4 acres; the size increases to around 0.8 acres at 50°N (Prins et al. 2001). The GOES, WF_ABBA has identified fires in South America less than 2.5 acres in size (Prins et al. 1998; Feltz et al. 2003). In Quebec, Canada, the algorithm has identified fires on the order of 5–7 acres (Prins et al. 2001).

WF_ABBA output were reproduced for the large Colorado fires discussed in this paper. Figure 16 shows the *GOES-11* WF_ABBA output centered over north-central Colorado on 8 June 2002 at 2315, 2320, 2325, and 2345 UTC. The Hayman fire shows up as a low probability fire pixel in the 2320 UTC image. At 2345 UTC it is characterized as a (cloudy) fire pixel. In this case a low probability fire pixel was the initial indication of the fire. Figure 17 shows several of the large Colorado wildland fires on the afternoon of 9 June 2002. The Missionary Ridge fire first appeared on WF_ABBA at 2055 UTC, which is the same time it became evident in the channel 2 imagery. However, notice how clearly the fires are portrayed on the output graphic. This clarity can help alleviate some of the perception problems discussed earlier.

8. Concluding remarks

The current GOES imaging channels provide a number of potentially powerful tools for use in the detection of vigorously burning wildland fires. However, there are several factors that can work against their efficient usage in the present operational environment. These factors include limited time resolution, relatively coarse spatial resolution, and delays in data delivery. The current system provides a partial solution to the first and third of these in the form of RSO—a special imaging schedule that can be activated by any National Weather Service office for any situation it deems important. The RSO schedule doubles the number of images received each hour and transfers the imagery onto AWIPS nearly three

FIG. 15. Photos from the Colorado Department of Health and Environment Web cam in downtown Denver. Times shown are (top) 1306 and (bottom) 1606 local daylight time (1906 and 2206 UTC). The images illustrate the effects of the arrival of the smoke plume in the Denver metro area by late afternoon.

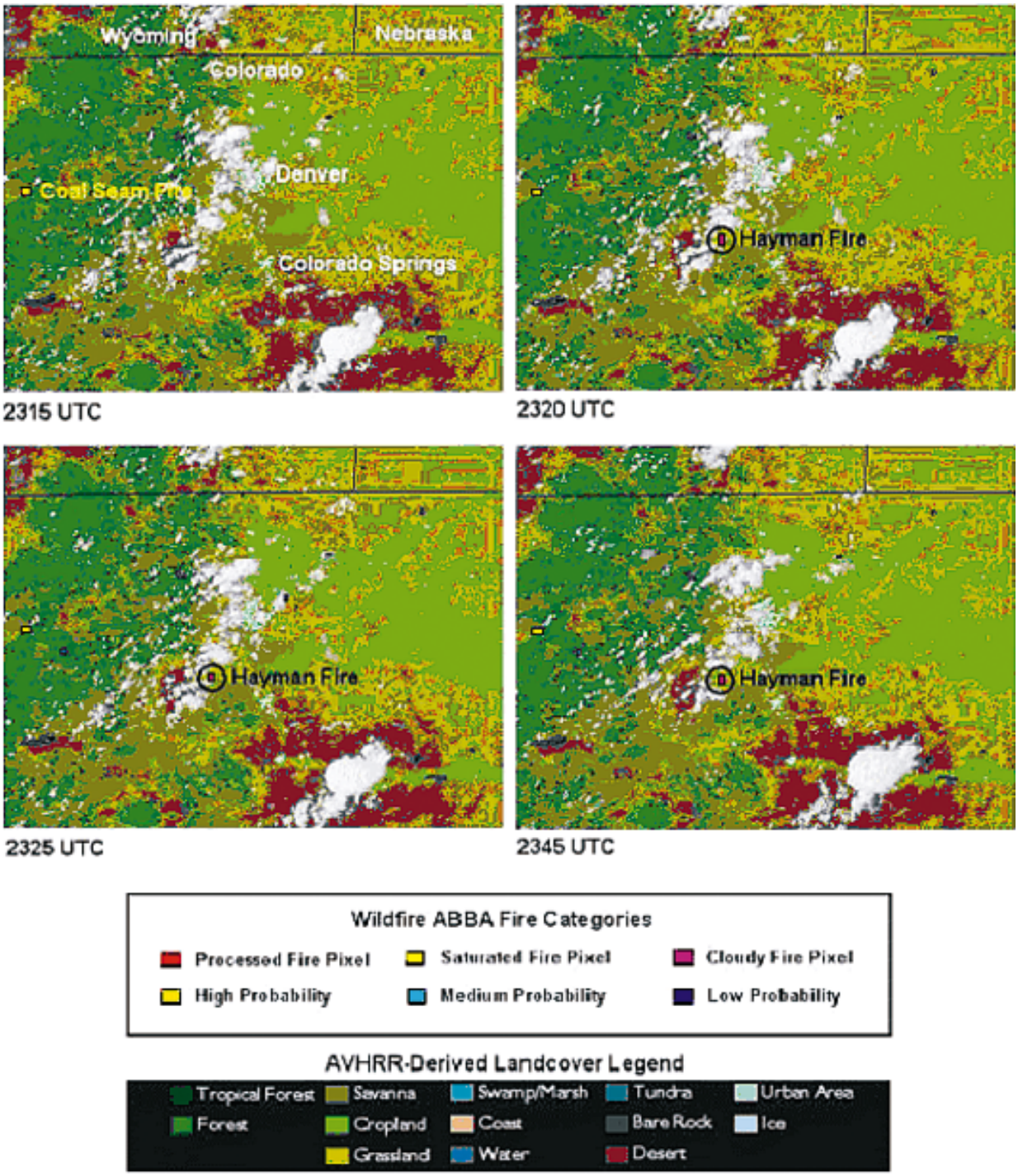

FIG. 16. *GOES-11* WF_ABBA fire product for 2315, 2320, 2325, and 2345 UTC on 8 Jun 2002. Images are centered over central Colorado. The WF_ABBA first detected the Hayman fire as a low probability fire pixel in the 2320 UTC image. At 2345 UTC it was characterized as a cloudy fire pixel. The image is a composite of WF_ABBA output and a color-enhanced image from the AVHRR Global Land Cover Characteristics (GLCC) database (information online at http://edcdaac.usgs.gov/glcc/glcc.html).

times more quickly. Plans for the next generation of geostationary satellites include operating the imaging instruments in a routine 5-min scanning mode. This more frequent imaging will eliminate the need for special RSO scheduling. Furthermore, the new generation of GOES instruments will have infrared resolutions of 1 km $\times$ 2 km, allowing for the detection of much smaller wildland fires.

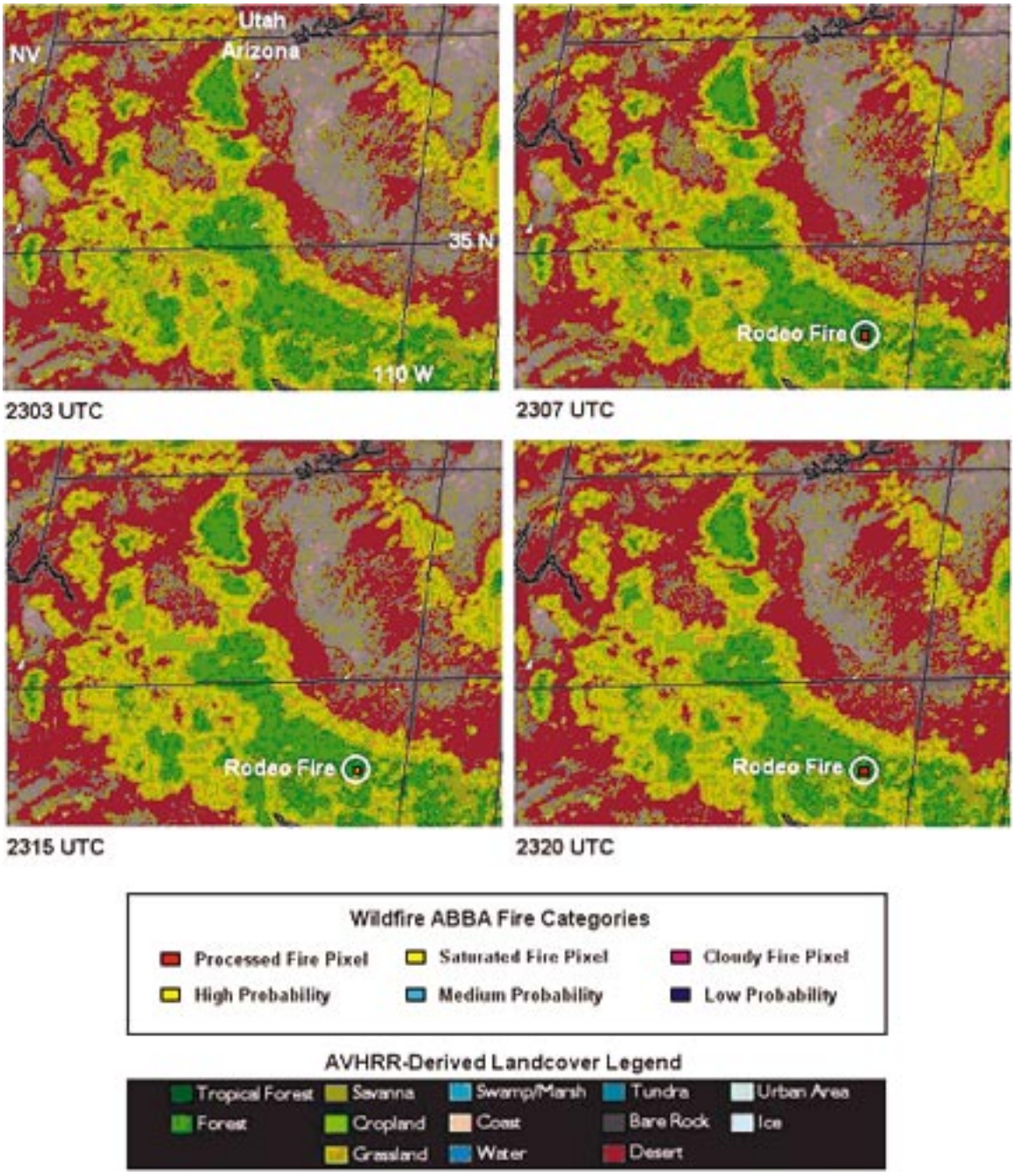

FIG. 17. Same as in Fig. 16 except image times are 1934, 2055, 2320, and 2325 UTC on 9 Jun 2002. Images are centered over southwest Colorado.

Within the next 1–2 yr, the full WF_ABBA fire detection algorithm will be made available for viewing within minutes of image scan time—including those images transmitted during RSO. With the algorithms that search for fires among several imaging channels, statistical checks that eliminate false alarms, and rapid product turnaround time, the success in remote detection of wildland fires is expected to increase dramatically.

Acknowledgments. A portion of the research presented in this study was performed under NOAA Grant NA67RJ0152. The authors wish to thank CIRA reviewers Dr. Mark DeMaria, Dr. Bernadette Connell, and Mr. Jack Dostalek, along with Dr. Phillip Bothwell (NOAA/SPC) and two anonymous reviewers, for their many insightful comments on various drafts of this manuscript.

REFERENCES

Bailey, A. W., and M. L. Anderson, 1980: Fire temperatures in grass, shrub and aspen communities in central Alberta. *J. Range Manage.*, **33,** 37–40.

Dozier, J., 1981: A method for satellite identification of surface temperature fields of sub-pixel resolution. *Remote Sens. Environ.*, **11,** 221–229.

Feltz, J. M., M. Moreau, E. M. Prins, K. McClaid-Cool, and I. F. Brown, 2003: Recent validation studies of the GOES Wildfire Automated Biomass Burning Algorithm (WF_ABBA) in North and South America. Preprints, *Second Int. Wildland Fire Ecology and Fire Management Congress*, Orlando, FL, Amer. Meteor. Soc., CD-ROM, P7.3.

Flannigan, M. D., and T. H. Vonder Haar, 1986: Forest fire monitoring using NOAA satellite AVHRR. *Can. J. For. Res.*, **16,** 975–982.

Matson, M., and J. Dozier, 1981: Identification of sub-resolution high temperature sources using a thermal IR sensor. *Photogramm. Eng. Remote Sens.*, **47,** 1311–1318.

Menzel, W. P., and J. F. W. Purdom, 1994: Introducing GOES-I: The first of a new generation of geostationary operational environmental satellites. *Bull. Amer. Meteor. Soc.*, **75,** 757–781.

——, and E. M. Prins, 1996: Monitoring biomass burning with the new generation of geostationary satellites. *Biomass Burning and Global Change*, J. S. Levine, Ed., The MIT Press, 56–64.

Prins, E. M., and W. P. Menzel, 1992: Geostationary satellite detection of biomass burning in South America. *Int. J. Remote Sens.*, **13,** 2783–2799.

——, and ——, 1994: Trends in South American biomass burning detected with the GOES visible infrared spin scan radiometer atmospheric sounder from 1983 to 1991. *J. Geophys. Res.*, **99,** 16 719–16 735.

——, J. M. Feltz, W. P. Menzel, and D. E. Ward, 1998: An overview of GOES-8 diurnal fire and smoke results for SCAR-B and the 1995 fire season in South America. *J. Geophys. Res.*, **103** (D24), 31 821–31 836.

——, J. Schmetz, L. Flynn, D. Hillger, and J. Feltz, 2001: Overview of current and future diurnal active fire monitoring using a suite of international geostationary satellites. *Global and Regional Wildfire Monitoring: Current Status and Future Plans*, F. J. Ahern, J. G. Goldammer, and C. O. Justice, Eds., SPB Academic, 145–170.

——, C. C. Schmidt, J. M. Feltz, J. S. Reid, D. L. Westphal, and K. Richardson, 2003: A two-year analysis of fire activity in the Western Hemisphere as observed with the GOES Wildfire Automated Biomass Burning Algorithm. Preprints, *12th Conf. on Satellite Meteorology and Oceanography*, Long Beach, CA, Amer. Meteor. Soc., CD-ROM, P2.28.

Weaver, J. F., J. F. W. Purdom, and T. L. Schneider, 1995: Observing forest fires with the *GOES-8*, 3.9-μm imaging channel. *Wea. Forecasting*, **10,** 803–808.